JPn Neuroscience
The Journal of Physiology

J Physiol 590.22 (2012) pp 5861–5875

Altered pallido-pallidal synaptic transmission leads to aberrant firing of globus pallidus neurons in a rat model of Parkinson's disease

Cristina Miguelez[1,2], Stéphanie Morin[1,2], Audrey Martinez[1,2], Michel Goillandeau[1,2], Erwan Bezard[1,2], Bernard Bioulac[1,2] and Jérôme Baufreton[1,2]

[1] *Univ. de Bordeaux, Institut des Maladies Neurodégénératives, UMR 5293, F-33000 Bordeaux, France*
[2] *CNRS, Institut des Maladies Neurodégénératives, UMR 5293, F-33000 Bordeaux, France*

Key points

- We used optogenetics approach to characterize the short-term plasticity of striato-pallidal (STR–GP) and pallido-pallidal (GP–GP) GABAergic synapses in rat brain slices.
- We show that only GP–GP (and not STR–GP) transmission is augmented by chronic dopamine depletion.
- Finally, we report that altered GP–GP synaptic transmission promotes neuronal synchronization and rebound bursting in globus pallidus neurons.
- Our results support the conclusion that maladaptive GP–GP GABAergic transmission is likely to be a key underlying factor of the pathological activity in the globus pallidus observed in Parkinson's disease.

Abstract The pattern of activity of globus pallidus (GP) neurons is tightly regulated by GABAergic inhibition. In addition to extrinsic inputs from the striatum (STR–GP) the other source of GABA to GP neurons arises from intrinsic intranuclear axon collaterals (GP–GP). While the contribution of striatal inputs has been studied, notably its hyperactivity in Parkinson's disease (PD), the properties and function of intranuclear inhibition remain poorly understood. Our objective was therefore to test the impact of chronic dopamine depletion on pallido-pallidal transmission. Using patch-clamp whole-cell recordings in rat brain slices, we combined electrical and optogenetic stimulations with pharmacology to differentiate basic synaptic properties of STR–GP and GP–GP GABAergic synapses. GP–GP synapses were characterized by activity-dependent depression and insensitivity to the D_2 receptor specific agonist quinpirole and STR–GP synapses by frequency-dependent facilitation and quinpirole modulation. Chronic dopamine deprivation obtained in 6-OHDA lesioned animals boosted the amplitude of GP–GP IPSCs but did not modify STR–GP transmission and increased the amplitude of miniature IPSCs. Replacement of calcium by strontium confirmed that the quantal amplitude was increased at GP–GP synapses. Finally, we demonstrated that boosted GP–GP transmission promotes resetting of autonomous activity and rebound-burst firing after dopamine depletion. These results suggest that GP–GP synaptic transmission (but not STR–GP) is augmented by chronic dopamine depletion which could contribute to the aberrant GP neuronal activity observed in PD.

(Resubmitted 20 July 2012; accepted 10 August 2012; first published online 13 August 2012)
Corresponding author J. Baufreton: Institut des Maladies Neurodégénératives, UMR 5293, F-33000 Bordeaux, France. Email: jerome.baufreton@u-bordeaux2.fr

Abbreviations GP, globus pallidus; GP–GP, pallido-pallidal; IPSC, inhibitory postsynaptic current; IPSP, inhibitory postsynaptic potential; 6-OHDA, 6-hydroxydopamine; PD, Parkinson's disease; STN, subthalamic nucleus; STD, short-term depression; STF, short-term facilitation; STP, short-term plasticity; STR–GP, striato-pallidal.

DOI: 10.1113/jphysiol.2012.241331

Introduction

The GABAergic globus pallidus (GP) is centrally positioned in the basal ganglia circuitry (Smith *et al.* 1998). It receives, processes and distributes cortico-striatal information to the entire network through its widespread axonal projections (Sato *et al.* 2000), thereby influencing basal ganglia nuclei output during voluntary movement-related tasks (Mink & Thach, 1991).

The *in vivo* activity of GP neurons is governed by the activity of the reciprocally connected glutamatergic sub-thalamic nucleus (STN) (Magill *et al.* 2000; Goldberg *et al.* 2003) as well as by inhibitory GABAergic inputs. Extrinsic inputs are provided by the striatal medium spiny neurons (MSN) from the indirect pathway and intrinsic inputs by intranuclear axon collaterals. Striato-pallidal (STR–GP) synapses representing 80–90% of dendritic synaptic boutons (Kita, 1994) play a critical function in the integration of convergent excitatory inputs from the STN (Smith *et al.* 1998). Pallido-pallidal (GP–GP) collaterals synapses, which account for ∼10% of the total number of GABAergic synapses, are mainly restricted to the soma and primary dendrites of GP neurons (Kita, 1994; Sadek *et al.* 2007) and are ideally positioned to exert a powerful control over action potential initiation and to pattern neighbouring GP neuron activity.

In a dopamine-depleted Parkinson-like condition, GP cells show greater propensity to fire in bursts (Filion & Tremblay, 1991) and pallidal neuron synchronisation increases (Nini *et al.* 1995). The mechanisms by which these changes in the pattern of GP neuron activity occur in PD are not fully understood, and hence the need to study dopamine modulation of pallidal synaptic transmission.

The STR–GP pathway is regulated by presynaptic D_2-like receptors (Cooper & Stanford, 2001). Moreover, chronic dopamine depletion leads to an enlargement of STR–GP synapses in the GP (Ingham *et al.* 1997) and an increased firing of STR–GP neurons (Kita & Kita, 2011) suggesting a hyperactive indirect pathway in PD. GP–GP synapses have not been studied in detail, but it has been suggested (Terman *et al.* 2002) that balanced inhibition between STR–GP and GP–GP pathways is essential for normal information processing by GP neurons and for preventing the development of pathological oscillatory activity in the GP–STN network observed in PD (Magill *et al.* 2001).

Our objective was thus to determine the impact of dopamine deprivation on the properties of STR–GP and GP–GP synapses using electro-physiological, pharmacological and optogenetic approaches.

Methods

Ethical approval

Sprague–Dawley rats were housed under a 12:12 light–dark cycle with food and water provided *ad libitum*. Every effort was made to minimize animal suffering and to use the minimum number of animals possible. Experimental procedures were conducted in accordance with institutional guidelines and the European Communities Council Directive dated 24 November 1986 (86/6091EEC).

6-Hydroxydopamine lesion

Rats (P17–19) were anaesthetized with ketamine (75 mg kg^{-1}) and xylazine (10 mg kg^{-1}) and mounted on a Kopf stereotaxic frame. According to our established procedures (Miguelez *et al.* 2011*b*), 2 μl of 6-OHDA (4 μg μl^{-1}) was infused at a rate of 0.5 μl min^{-1} into the right medial forebrain bundle (relative to bregma: AP: −2.4 mm, ML: −1.2 mm, DV: −7.4 and −7.9 mm, 1 μl was injected in each coordinate). After each injection, the needle was left in place for an additional 2–4 min to allow the toxin to diffuse into the structure before being slowly retracted. For sham animals, vehicle was injected in the same coordinates. Thirty minutes before surgery, desipramine (20 mg kg^{-1}, I.P.) was administered to avoid damage of the noradrenergic system. Rats were killed for recordings 2–3 weeks after this operation.

Cylinder test

To assess the degree of motor impairment produced by dopamine depletion, forelimb use asymmetry was evaluated using the cylinder test (Schallert *et al.* 2000; Cenci & Lundblad, 2007; Miguelez *et al.* 2011*a*). The screening of the lesion was evaluated 2 weeks after surgery when the pathological activity is considered stabilized (Vila *et al.* 2000). Briefly, rats were placed individually in a 20 cm diameter glass cylinder and allowed to move freely for 5 min. During this time, the number of wall placements performed with the ipsilateral or contralateral forelimb to the lesion side were counted and expressed as a percentage of the total number of wall contacts.

In the cylinder test, the dopamine depleted rats showed significant severe forelimb use asymmetries for wall exploration ($P < 0.001$, Student's t test), performing 17.6 ± 1.6% wall contacts with the paw contralateral to the lesion and 82.4 ± 1.6% with the ipsilateral one. In contrast, sham animals performed equally with both paws (50.7 ± 1.3% and 49.3 ± 1.3% with ipsilateral and contra-lateral paw, respectively). The forelimb impairment of the contralateral paw to the lesion site was significantly

increased in 6-OHDA animals compared to the sham group ($P < 0.001$, Student's t test), and therefore forelimb asymmetry was consistent with the dopaminergic denervation (Supplemental Fig. 1*E*).

Channelrhodopsin-2 transfection of striatal and pallidal cells

The cation channel channelrhodopsin-2 (ChR2) was transfected in striatal cells using a lentiviral vector, including a yellow fluorescent protein (YFP) reporter, under the CaMKIIα promoter (pLenti-CAMKIIα-hChR2-EYFP-WPRE, www.optogenetics.org). Viral DNA was generously provided by Karl Deisseroth (Stanford University). For transfecting GP neurons, adeno associated viral vector including YFP reporter under hSyn promoter (pAAV-hSyn-hChR2(H134R)-EYFP, Penn Vector Core, http://www.med.upenn.edu/gtp/vectorcore/Catalogue.shtml#VectorCatalog) was used. Sprague–Dawley rats (P15–19) were anaesthetized with ketamine/xylazine and placed in a stereotaxic frame. The two vectors used in this study have been characterized previously to have a restricted diffusion capacity and a limited nerve terminal uptake (for review see Davidson & Breakefield, 2003; Zhang *et al.* 2010). Indeed, we found that viral transfection was restricted to the cell bodies as no fluorescence was observed in presynaptic structures (e.g. the cortex or the thalamus for striatal injections and the striatum for pallidal injections). For striatal transfection, four injections of 1 μl were performed in the right striatum (relative to bregma: AP: +0.8 mm, ML: −2.6 mm, DV: −4.2 and −3.4 mm and AP: +0.0 mm, ML: −3.0 mm, DV: −4.6 and −3.8 mm). For transfection in the GP, two injections of 0.5 μl were placed in the right GP (relative to bregma: AP: −0.4 mm, ML: −2.4 mm, DV: −5.5 and −6.0 mm). After each injection the needle was left in place for an additional 2–4 min and then slowly retracted (Ahmed *et al.* 2010).

Electrophysiology

Slice preparation. Ninety-two animals (P30–45, at the time of the experiment) were used for the electrophysiological recordings. Animals were anaesthetized with ketamine/xylazine and perfused transcardially with ice-cold modified artificial cerebrospinal fluid (ACSF), equilibrated with 95% O_2–5% CO_2, containing (in mM): 230 sucrose, 26 $NaHCO_3$, 2.5 KCl, 1.25 NaH_2PO_4, 0.5 $CaCl_2$, 10 $MgSO_4$, and 10 glucose. The brain was removed, submerged in ice-cold modified ACSF and sectioned into 350 μm thick slices with a vibrating blade microtome (VT1200S; Leica Microsystems, Germany) in the parasagittal or coronal plane. Slices containing the GP were then stored in ACSF equilibrated with 95% O_2–5% CO_2, and containing (in mM): 126 NaCl, 26 $NaHCO_3$, 2.5 KCl, 1.25 NaH_2PO_4, 2 $CaCl_2$, 2 $MgSO_4$ and 10 glucose.

Whole-cell voltage-clamp and current-clamp recordings. Single slices were transferred to a recording chamber, which was perfused continuously with ACSF heated to 32–34°C, equilibrated with 95% O_2–5% CO_2, and containing (in mM): 126 NaCl, 26 $NaHCO_3$, 3 KCl, 1.25 NaH_2PO_4, 1.6 $CaCl_2$, 1.5 $MgSO_4$ and 10 glucose. GP or striatal neurons were visualized with infrared gradient contrast video microscopy (Eclipse workstation; Nikon, Japan) and a ×63 water-immersion objective (E600FN, Nikon, Japan). Somatic patch clamp recordings were made using pipettes (impedance, 3–6 MΩ) prepared from borosilicate glass capillaries (G150–4; Warner Instruments, Hamden, CT, USA) with a micropipette puller (P-97; Sutter Instruments, Novato, CA, USA) and were filled with (in mM): 135 KCl, 3.6 NaCl, 1 $MgCl_2$, 10 Hepes, 5 QX-314, 0.1 Na_4EGTA, 0.4 Na_3GTP, 2 $Mg_{1.5}$ATP and 0.02 Alexa fluor-568 (pH 7.2, 290 mosmol l^{-1}) for the recording of evoked IPSCs in voltage clamp mode or (in mM): 120 potassium gluconate, 10 KCl, 10 NaCl, 11 EGTA, 10 Hepes, 1 $CaCl_2$, 0.4 Na_2GTP, 2 $Mg_{1.5}$ATP and 0.02 Alexa fluor-568 (pH 7.2, 290 mosmol l^{-1}) for whole-cell current clamp recordings. Perforated-patch current-clamp recordings were performed using (in mM): 106 K-$MeSO_4$, 25 KCl, 1 $MgCl_2.6H_2O$, 0.1 $CaCl_2$, 10 Hepes, 1.1 Na_4EGTA, 0.4 Na_2GTP and 2 $Mg_{1.5}$ATP. With this pipette solution, reversal potential for chloride is ∼−40 mV allowing immediate detection of accidental break-in by a change in the polarity of $GABA_A$-receptor mediated IPSCs from hyperpolarizing to depolarizing. Gramicidin D (Sigma-Aldrich, France) was added to the patch solution at a concentration of ∼15 μg ml^{-1}. The mean values for series resistances were 59.8 ± 8.4 MΩ ($n = 12$) and 63.6 ± 5.6 MΩ ($n = 13$) for control and 6-OHDA recordings, respectively.

Data were recorded using a Multiclamp 700B amplifier controlled by Clampex 9.0 (Molecular Devices, Sunnyvale, CA, USA). Signals were digitized at 20 kHz and low-pass filtered at 6 kHz, respectively. Whole-cell voltage clamp recordings with KCl-filled electrodes and perforated-patch current clamp recordings with $KMSO_4$-filled electrodes were corrected for a junction potential of 4 mV and whole-cell current-clamp recordings for a junction potential of 5 mV (Barry, 1994). Evoked $GABA_A$R-mediated IPSCs (eIPSCs) were recorded at a holding potential of −60 mV (after junction potential correction). In voltage clamp experiments, series resistance was monitored by a step of −5 mV at the end of each recording. Data were discarded when the series resistance increased by >20%. All synaptic recordings in voltage-clamp were performed in the presence of 1 μM

(2*S*)-3-[(1*S*)-1-(3,4-dichlorophenyl)ethyl]amino-2-hydroxypropyl)(phenylmethyl)phosphinic acid (CGP5 5845; Tocris Bioscience, Bristol, UK), 50 μM D-(−)-2-amino-5-phosphonopentanoic acid (APV; Ascent Scientific, Cambridge, UK), 20 μM 6,7-dinitroquinoxaline-2,3-dione (DNQX; Ascent Scientific) to block $GABA_B$, NMDA and AMPA/kainate receptors, respectively. In some cases, 20 μM 4-[6-imino-3-(4-methoxyphenyl) pyridazin-1-yl] butanoic acid hydrobromide (GABAzine/SR-95531) was applied to confirm that the remaining synaptic events were indeed sensitive to a selective $GABA_A$ receptor antagonist. Measurements of the reversal potential of $GABA_A$ receptor-mediated IPSP ($EGABA_A$) were performed as previously described (Bevan *et al.* 2000).

Evoked and miniature IPSCs. Single IPSCs or trains of IPSCs were evoked at 1, 10 and 20 Hz by bipolar electrical stimulation of the striatum in parasagittal slices or the GP in coronal slices, respectively (0.05–0.7 mA; ISO-Flex, A.M.P.I., Jerusalem, Israel) using a custom-built matrix of 20 stimulation electrodes with 190 μm spacing between each electrode (MX54CBWMB1; Frederick Haer Company, Bowdoinham, ME, USA). The stimulation intensities were adjusted in the experiments run on coronal and parasagittal slices and in recordings performed in control and dopamine-depleted slices; the mean stimulation intensity was not significantly different between each conditions (parasagittal control; intensity = 244 ± 27.56 μA, $n = 20$; parasagittal 6-OHDA; intensity = 230.6 ± 39.18 μA, $n = 9$; $P = 0.866$, Mann–Whitney U test; coronal control; intensity = 216.3 ± 29.92, $n = 15$; coronal 6-OHDA; intensity = 195.3 ± 32.89 μA, $n = 17$; $P = 0.473$, Mann–Whitney U test).

Action potential-independent miniature IPSCs (mIPSCs) were recorded at a holding potential of –60 mV in presence of 1 μM of tetrodotoxin (TTX) in coronal slices obtained from control and dopamine-depleted animals.

Sr^{2+}-induced asynchronous release experiments. In order to probe quantal properties of facilitating (STR–GP) and depressing (GP–GP) synapses, extracellular calcium was replaced by strontium and each pathway was studied in isolation in either parasagittal or coronal slices, respectively. With a bath solution containing 3.2 mM Sr^{2+} (and 0 mM Ca^{2+}), Sr^{2+} enters through Ca^{2+} channels and causes asynchronous exocytosis of vesicles not fused during the initial event, possibly because Sr^{2+} does not modulate Ca^{2+}-sensor proteins involved in the synchronization of vesicular release (Fioravante & Regehr, 2011). Under this experimental condition, quantal-like events (qIPSCs) could be recorded and analysed to characterize properties of facilitating STR–GP synapses (recorded in parasagittal slices) and depressing (recorded in coronal slices) GP–GP synapses.

Cell-attached voltage-clamp recordings

Cell-attached recordings were performed prior to establishment of whole-cell recording in presence of glutamatergic synaptic transmission and $GABA_B$ receptor blockers (APV, DNQX and CGP55845). These recordings (2–4 min in duration) were performed at a holding potential of 0 mV after the stable establishment of the gigaseal.

Optogenetic cell control

Two weeks after stereotaxic viral transfection, when ChR2 expression was considered stable, electrophysiological recordings were carried out. The optical set-up consisted of an optic fibre connected to a blue laser with a wavelength of 473 nm (Optotronics, Mead, CO, USA) with a maximum output of 150 mW. An optical fibre was positioned above an area with good striatal or pallidal transfection, as observed under a fluorescence microscope. A continuous or blinking blue light was flashed onto the transfected area. For studying STR–GP or GP–GP synaptic transmission, trains of 1 ms optical stimulation at 1, 10 and 20 Hz were performed in the striatum or the GP, respectively, and $GABA_A$-mediated IPSCs were recorded in the GP. In GP ChR2-expressing slices, the ChR2 photocurrent was revealed by application of GABAzine. We only included in this study the recordings in which direct activation of ChR2 in recorded neurons was less than 10% of the total current (see Supplemental Fig. 2*G* and *H*). Therefore, to normalized IPSC amplitude, the residual current recorded in GABAzine was subtracted from the total current evoked by the light flashes. Specific expression of ChR2 in the GP was checked by recording striatal MSN neurons in current-clamp configuration with the optical stimulation delivered in the vicinity of the recorded cells. Flashes of light never induced depolarization of the membrane potential of MSN neurons, suggesting that transfection of ChR2 was restricted to the GP (Supplemental Fig. 2*K* and *L*). As well, GP neurons never responded to light stimulation delivered in the GP when ChR2 was injected in the striatum (Supplemental Fig. 2*I* and *J*).

Immunohistochemistry

Tyrosine hydroxylase (TH) immunostaining. As described previously (Miguelez *et al.* 2011*b*), slices fixed overnight in 4% paraformaldehyde were immersed in phosphate buffered saline (PBS) and re-sectioned in 50 μm slices using a cryostat (Leica CM3000, Leica Microsystems).

After inactivation of endogenous peroxidases (3% H_2O_2 in PBS for 30 min), slices were blocked in 1% bovine serum albumin (BSA) in PBS containing 0.3% Triton X-100 for 30 min. Thereafter, sections were incubated in primary antibody (1:10000 monoclonal anti-TH; MAB318, Chemicon, Temecula, CA, USA) overnight. After rinsing, the sections were treated with the secondary antibody (1:1000 biotinylated horse anti-mouse IgG; Vector Laboratories, Burlingame, CA, USA) for 90 min. Both immunoreagents were diluted in PBS containing 1% BSA, 0.3% Triton X-100. Finally, sections were incubated in avidin–biotin peroxidase complex (1:500; Vector Laboratories) for 60 min and immunoreactivity was revealed using diaminobenzidine tetrahydrochloride (Vector Laboratories). Sections were rinsed, mounted on gelatine-coated slides and coverslipped in Vectamount (Vector Laboratories). The entire procedure was performed at room temperature under gentle agitation.

Tyrosine hydroxylase optical density and stereological counting of substantia nigra compacta dopaminergic neurons

Sections containing the striatum were placed on an optical bench and scanned for further processing. Mean optical density was analysed using the Mercator image analysis system (Explora Nova, La Rochelle, France). Mean optical density values were corrected for background staining. TH optical density levels were expressed as a percentage of the values from the intact side.

Stereological cell counting was performed as described previously (Bezard *et al.* 1997; Gross *et al.* 2003). Fifty-micrometer free-floating mesencephalic serial sections were processed for TH immunohistochemistry and then counterstained with cresyl violet (Nissl staining). Cell counts were performed in six regularly spaced sections along the substantia nigra pars compacta (SNc) using a computer-based image analyser (Explora Nova). Unbiased stereological techniques were used to estimate cell numbers in the SNc (West, 1999).

Optical density and stereological accounting were performed in slices containing striatum and the SNc, respectively, from sham (Supplemental Fig. 1*A* and *C*) and 6-OHDA lesioned animals (Supplemental Fig. 1*B* and *D*). Animals with unilateral 6-OHDA infusions included in the study showed 97 ± 2.04% reduction in TH-fibre density in the striatum on the side ipsilateral to the lesion. The precision of the method to quantify the degree of dopaminergic denervation was confirmed by the existence of a significant positive correlation between the number of cells in the substantia nigra compacta (SNc) and the striatal optical density of the side ipsilateral to the lesion ($r = 0.96$, $P < 0.001$, Supplemental Fig. 1*F*).

YFP immunostaining. Slices containing the striatum were fixed overnight and then rinsed in PBS and blocked by 1% bovin serum albumin (BSA) in PBS containing 0.3% Triton X-100 for 90 min. Sections were incubated in primary antibody (1:1000 anti-GFP, Invitrogen) overnight. After rinsing, the sections were treated with the secondary antibody (1:500 Alexa fluor 488 anti-rabbit; Invitrogen) for 2 h. Both immunoreagents were diluted in PBS containing 1% BSA, 0.3% Triton X-100. Thereafter, sections were rinsed, mounted on gelatine-coated slides and coverslipped in Vectashield (Vector Laboratories). Slices were observed and images were acquired under epifluorescence on a macroscope (Nikon, AZ100M).

Analysis and statistics

The amplitude of the evoked IPSCs (eIPSCs) was calculated from the baseline preceding the stimulation and baseline current previous to each individual stimulation artefact with Clampfit 9.2 (Molecular Devices) and was represented in absolute amplitude in the text and corresponding figures. Stimulus artefacts were removed off-line for clarity. Analyses of mIPSCs recorded in the presence of TTX and qIPSCs recorded in the presence of Sr^{2+} in the ACSF were performed on at least 200 events with software developed in-house. Cumulative distributions were compared using the Kolmogorov–Smirnov test (K–S test) and were considered to be significantly different when $P < 0.01$. Paired and unpaired data were compared using a non-parametric Wilcoxon's signed rank (WSR) test and Mann–Whitney (MW) *U* test, respectively, unless otherwise stated in the text. Significance was considered at $P < 0.05$. Data are represented as group means ± the standard error of the mean (SEM).

Results

Electrophysiological characterization of two types of GABAergic synapses in the globus pallidus

First we wanted to characterize the short-term plasticity (STP) of putative STR–GP and GP–GP synapses under control conditions. $GABA_A$ receptor-mediated synaptic transmission was explored using trains of electrical stimuli at 1 Hz, 10 Hz and 20 Hz. In parasagittal slices which preserve at least some STR–GP connections we found two types of STP when electrical stimulation was delivered in the striatum. In half of the recordings (23/44 neurons), frequency-dependent STP was a pronounced short term facilitation (STF) during trains of stimulation at 1, 10 and 20 Hz (Fig. 1*A* and *D*). In the remaining recordings (21/44 neurons), synaptic responses were governed by a moderate short-term depression (STD) with ratios of 0.91 ± 0.19,

0.83 ± 0.08 and 0.92 ± 0.15 at 1, 10 and 20 Hz, respectively ($n = 8$, 21, 12 at 1, 10 and 20 Hz; Fig. 1*B* and *E*).

In coronal slices, electrical stimulations were performed in the GP, at a distance ranging from 50 to 200 μm from the recorded GP neurons. Most of the synaptic responses (79%) were characterized by STD with ratios of 0.78 ± 0.14, 0.85 ± 0.08 and 0.81 ± 0.09 at 1, 10 and 20 Hz, respectively ($n = 3$, 15 and 9 at 1, 10 and 20 Hz; Fig. 1*C* and *F*). The profiles of STD recorded in the parasagittal and coronal sections were similar (MW *U* test, $P > 0.05$). We made the hypothesis that they reflected the properties of the same population of GABAergic synapses, and thus the data were pulled. A comparison between facilitating and depressing responses then revealed significant differences in the amplitude of eIPSCs early in the train ($P < 0.001$, MW *U* test) but not at the end of the train ($P = 0.051$, MW *U* test) (Fig. 1*G*) whereas mean intensities of stimulation were similar. Most importantly, this was accompanied by significant differences in the frequency-dependent short-term dynamics of GABAergic transmission of depressing and facilitating responses ($P < 0.01$, Fig. 1*H*).

Specific activation of STR–GP and GP–GP synapses using optogenetics

In order to provide direct evidence regarding the identity of the depressing and facilitating synapses, we expressed the channelrhodopsin ChR2 in striatal or GP cells *via* local viral transfection (Fig. 2*A* and *B*) and used 473 nm light stimulations to evoke synaptic transmission (Cruikshank *et al.* 2010) (Fig. 2*C*). We tested that MSN and GP neurons' excitability was not altered by the expression of ChR2 and that brief flashes of light were able to reliably trigger single action potential in both neuronal types (see Supplemental Fig. 2*A–D*). In striatum ChR2-expressing slices, light stimulations evoked STF whereas in GP ChR2-expressing slices, light activated synapses showed STD (Fig. 2*C*, examples for 10 Hz) with STD profiles similar to those obtained by electrical stimulation (Fig. 2*C*; for comparison, see Fig. 1*H*). Light-evoked STR–GP IPSCs were completely abolished by GABAzine, confirming that the currents were mediated specifically by $GABA_A$ receptors (see Supplemental Fig. 2*E* and *F*). These data support the conclusion that the depressing responses recorded in parasagittal or coronal slices are those of a same type of synapses. They demonstrate that these are GP–GP synapses. They provide compelling evidence that STR–GP and GP–GP synaptic transmission possess distinct STP, the former being facilitating whereas the latter is depressing.

D_2 dopamine receptor modulation of pallidal GABAergic synapses

Modulation by presynaptic D_2 dopamine receptors of STR–GP synaptic transmission has been reported (Cooper & Stanford, 2001) but the effect of D_2R activation on STP of GP–GP synapses is unknown. Thus, since 10 Hz trains exemplified STP in all conditions examined, 10 Hz frequency trains of IPSCs were evoked in the presence of the D_2 agonist quinpirole. The amplitude of the initial IPSC of facilitating synapses was reduced

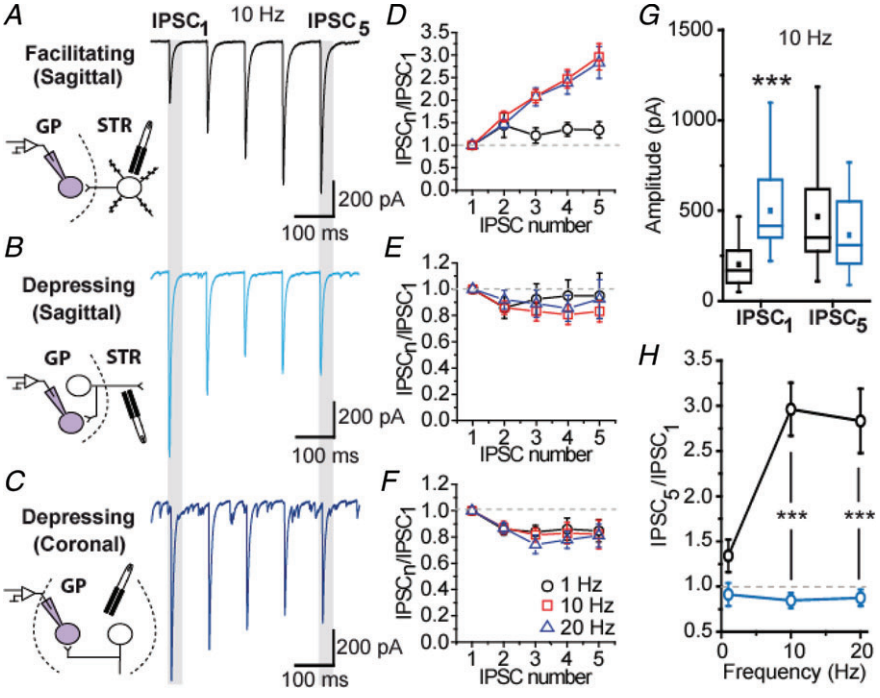

Figure 1. Short-term synaptic plasticity of STR–GP and GP–GP synapses under physiological conditions
A–C, examples of electrically evoked trains of IPSC at 10 Hz frequency. Drawings depict the putative synapses stimulated for each experimental condition. *D–F*, graphs showing normalized IPSC amplitude. *G*, graph showing the amplitude of the first and last IPSCs in the train at a frequency of 10 Hz. *H*, summary graph of the normalized amplitude of the last IPSC ($IPSC_5/IPSC_1$) of the train. ***$P < 0.001$ *vs.* facilitating synapse, MW *U* test.

by 51.5% in the presence of quinpirole ($P = 0.0078$, WSR test) (Fig. 3*A* and *B*) and was associated with a significant increase in synaptic facilitation shown by the augmentation of the $IPSC_5/IPSC_1$ ratio in the presence of quinpirole ($P = 0.015$, WSR test; Fig. 3*C*). This result indicates that the STR–GP synapse release probability (P_r) is modulated by presynaptic D_2R. In contrast, depressing IPSCs recorded in parasagittal and coronal slices were insensitive to quinpirole (Fig. 3*D*) since neither the amplitude of the initial IPSC ($P = 0.843$, WSR test; Fig. 3*E*) nor the normalized IPSCs were affected by the D_2R selective agonist ($P = 0.547$, WSR test; Fig. 3*F*). Quinpirole also failed to modulate light-evoked trains of IPSCs (Fig. 3*G* and *H*, $n = 4$) of GP neurons in GP ChR2-expressing slices, which confirms the insensitivity of depressing synapses to D_2R modulation (Fig. 3*H* and *I*).

Chronic dopamine depletion boosts GP–GP synaptic transmission

In order to test the impact of chronic dopamine depletion, we investigated the frequency-dependent STP in control and 6-OHDA-lesioned animals.

Surprisingly, STF at putative STR–GP synapses was not modified after 6-OHDA treatment suggesting that the mode of transmission of STR–GP facilitating synapses is not affected by chronic dopamine depletion (Fig. 4).

On the other hand we found that, at depressing synapses (whether recorded in parasagittal or coronal slices), IPSCs amplitude was significantly augmented in slices obtained from dopamine-depleted rats compared to control rats (Fig. 5*Aa–Bb*). This increase was present throughout the trains at 1, 10 and 20 Hz (Fig. 5*C*, example for 10 Hz). On average, the mean amplitude values measured for the last eIPSC of trains were significantly boosted by 67%, 70% and 62% at 1 Hz ($P = 0.044$, MW *U* test), 10 Hz ($P = 0.003$, MW *U* test) and 20 Hz ($P = 0.033$, MW *U* test) (Fig. 5*D*), respectively. This increase in evoked IPSCs amplitude cannot be attributed to a difference in stimulus intensities as the mean intensity values were not statistically different between the control and the 6-OHDA groups (see Methods). It did not alter STP dynamics as the normalized eIPSCs displayed the same degree of depression between the two groups at all frequencies (Fig. 5*E* and *F*). Furthermore, the lack of change in the paired-pulse ratio suggests that dopaminergic depletion-induced boosting of GP–GP synaptic transmission has a postsynaptic origin ($P > 0.05$ for all pairwise comparisons, MW *U* test) (Fig. 5*E* and *F*). To test this possibility, action potential-independent transmission was recorded in presence of 1 μM of TTX. Under these recording conditions, we found that mIPSCs amplitude was significantly augmented by 38% (Fig. 6*A–C* and *E*; $P = 0.015$, MW *U* test) whereas their frequency was not modified by dopamine depletion (Fig. 6*A*, *B*, *D* and *F*; $P = 0.43$, MW *U* test).

To further support our paired-pulse ratio data and our mIPSCs results, and probe quantal properties of depressing (GP–GP) synapses, extracellular calcium was substituted by strontium and GP–GP synaptic transmission was studied in isolation in coronal slices (see Methods). Quantal-like events were recorded and analysed to characterize the properties of depressing pallidal synapses (Fig. 7*A–D*). When Sr^{2+}-induced asynchronous release was recorded in slices from 6-OHDA lesioned animals, the frequency of qIPSC was unchanged ($P = 0.323$, MW *U* test, Fig. 7*C*). However, the amplitude of qIPSC was significantly increased (41% on average, $P = 0.023$, MW *U* test, Fig. 7*D*), which can account for the boosting of evoked synaptic transmission observed at

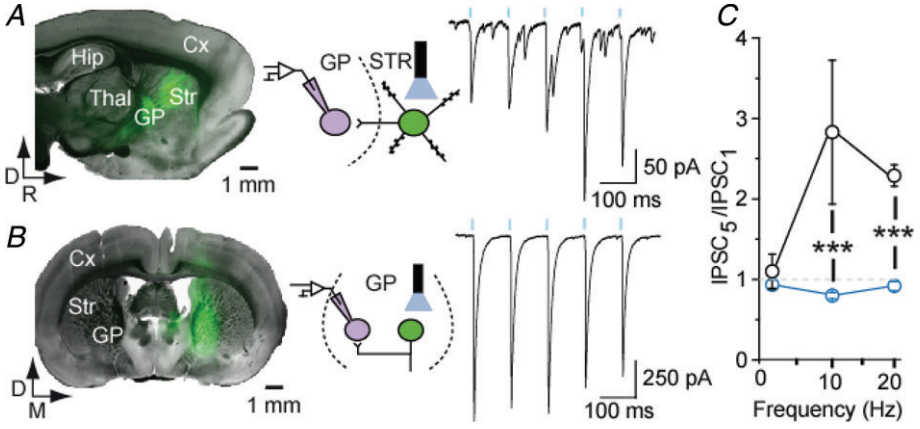

Figure 2. Optogenetic characterization of STR–GP and GP–GP synapses
A, parasagittal section showing ChR2-YFP expression in the striatum and a typical example of facilitating STR–GP responses elicited by 1 ms flashes of light (10 Hz) in the striatum ($n = 6$). *B*, coronal section showing ChR2 expression in GP and a typical depressing GP–GP train of IPSC delivered in GP ($n = 5$). *C*, summary graph of the normalized amplitude of the last IPSC of the train. ***$P < 0.001$ *vs.* facilitating synapse, MW *U* test.

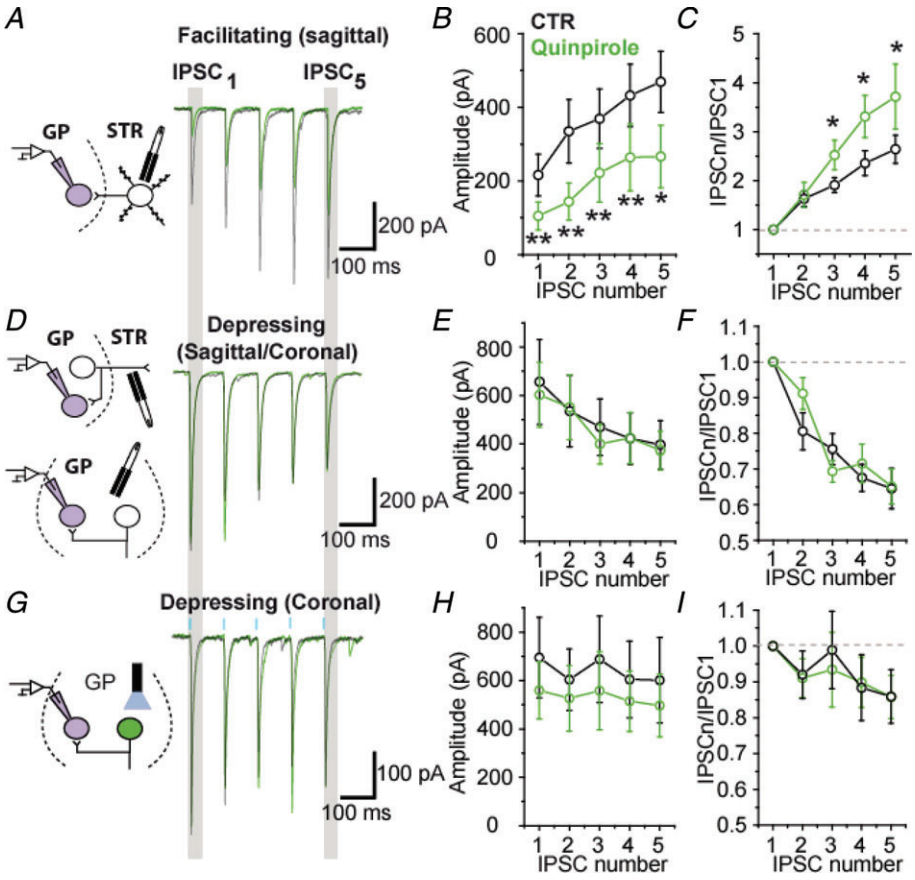

Figure 3. GP–GP synapses are not modulated by D_2 dopamine receptors
A, superimposed train of electrically-evoked IPSCs at 10 Hz in the absence (black) or presence of 2 μM quinpirole (green; grey in the print edition) in parasagittal slices. *B*, population graph showing a significant reduction in the IPSC amplitude by quinpirole at facilitating synapses. *C*, graph of normalized IPSCs showing a greater facilitation in the presence of quinpirole. *D–F*, same as *A–C* but for depressing synapses recorded in coronal or parasagittal slices. *G*, optically evoked train of GP–GP IPSC in coronal section at 10 Hz. *H* and *I*, summary graph showing the lack of modulation by the D_2 agonist on GP–GP synapses ($n = 4$). $^*P < 0.05$ and $^{**}P < 0.01$ *vs.* control, WSR test. Eight and four neurons were used in each group for electrical and optical stimulations, respectively.

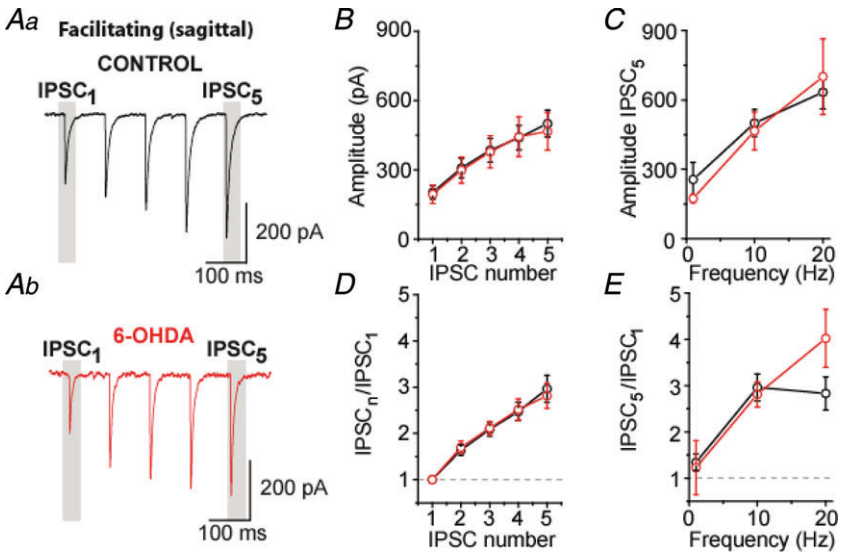

Figure 4. STR–GP synaptic transmission is not altered by dopamine depletion
A and *B*, examples of facilitating IPSCs at 10 Hz in control (*Aa*) and dopamine-depleted (*Ab*) slices recorded in parasagittal sections, respectively. *B*, population graph showing IPSCs amplitude at 10 Hz. *C*, population graph representing the magnitude of the last IPSC of the train. *D*, graph of normalized IPSCs at 10 Hz. *E*, normalized amplitude for the last IPSC of the train at 1, 10 and 20 Hz.

depressing synapses. Absence of change in the frequency and the amplitude of qIPSCs recorded in parasagittal slices (Fig. 7*E–H*) also supports that dopamine deprivation did not affect STP of putative STR–GP synapses. Altogether, these results demonstrate that chronic dopamine depletion alters GABAergic transmission at putative GP–GP depressing synapses without affecting the STR–GP pathway.

Impact of GP–GP transmission on the firing activity of pallidal neurons from dopamine-depleted animals

Chronic dopamine depletion has been reported to significantly reduce the excitability of GP neurons (Chan *et al.* 2011). Therefore, before addressing the impact of altered GP–GP GABAergic transmission on the pacemaking of GP neurons we first investigated modification of GP neuron firing rate in cell-attached and perforated-patch recordings in slices derived from control and dopamine-depleted animals. We found a significantly greater proportion of silent GP neurons after chronic dopamine depletion (control: 25.2%; 23 out of 91 neurons; 6-OHDA; 46.3%; 45 out of 97 neurons; $P = 0.0038$; Fischer's exact test; Fig. 8*A* and *B*). Despite this greater number of silent neurons, the average firing frequency was not statistically different between the control and the 6-OHDA groups when all the neurons were included in the analysis ($P = 0.292$; MW *U* test; Fig. 8*C*). This result suggested that silencing of GP neurons induced by dopamine depletion is compensated by a higher discharge frequency of the remaining active neurons. This was confirmed by the significant higher mean firing frequency of GP neurons recorded from 6-OHDA treated animals ($P = 0.004$; MW *U* test; Fig. 8*D*) when only active cells were included in the analysis.

The impact of putative GP–GP inputs on the activity of GP neurons was then analysed on 25 patch-perforated current clamp recordings (12 neurons in control conditions and 13 from 6-OHDA-treated rats) in coronal slices with $GABA_A$ inhibitory postsynaptic potentials (IPSPs) evoked by intra-pallidal electrical stimulation. $EGABA_A$ was not modified by dopamine depletion (Fig. 9*A* and *B*, $P = 0.289$, MW *U* test). Measurements at matching membrane potential (−65 mV) revealed a significant (+92%) increased in the amplitude of the IPSPs in dopamine-deprived conditions (Fig. 9*A* and *C*; $P = 0.039$, MW *U* test), in agreement with our voltage-clamp data. We then tested the effect of a single IPSP on autonomous discharge of GP neurons (only in neurons which were autonomously pacemaking). We found that the jitter of the post-IPSP action potential was significantly reduced in dopamine-depleted slices (Fig. 9*D* and *E*; $P = 0.03$, MW *U* test). This result suggests that GP–GP GABAergic transmission in dopamine-depleted animals favours synchronization of GP neuron activity.

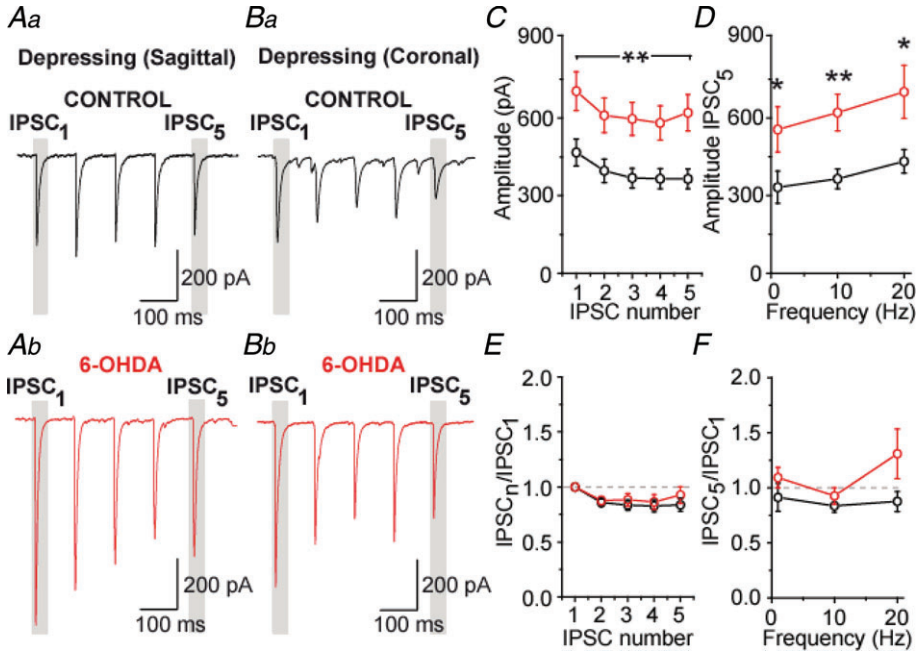

Figure 5. Dopamine depletion increases the amplitude of GP–GP IPSCs
A and *B*, examples of depressing IPSCs at 10 Hz in control (*Aa* and *Ba*) and dopamine-depleted (*Ab* and *Bb*) slices recorded in parasagittal and coronal plans, respectively. *C*, population graph showing a significant increase in IPSC amplitude after dopamine depletion at 10 Hz. *D*, population graph representing the magnitude of the last IPSC of the train. *E*, graph of normalized IPSCs at 10 Hz. *F*, normalized amplitude for the last IPSC of the train at 1, 10 and 20 Hz. $*P < 0.05$ and $**P < 0.01$ *vs.* control, MW *U* test.

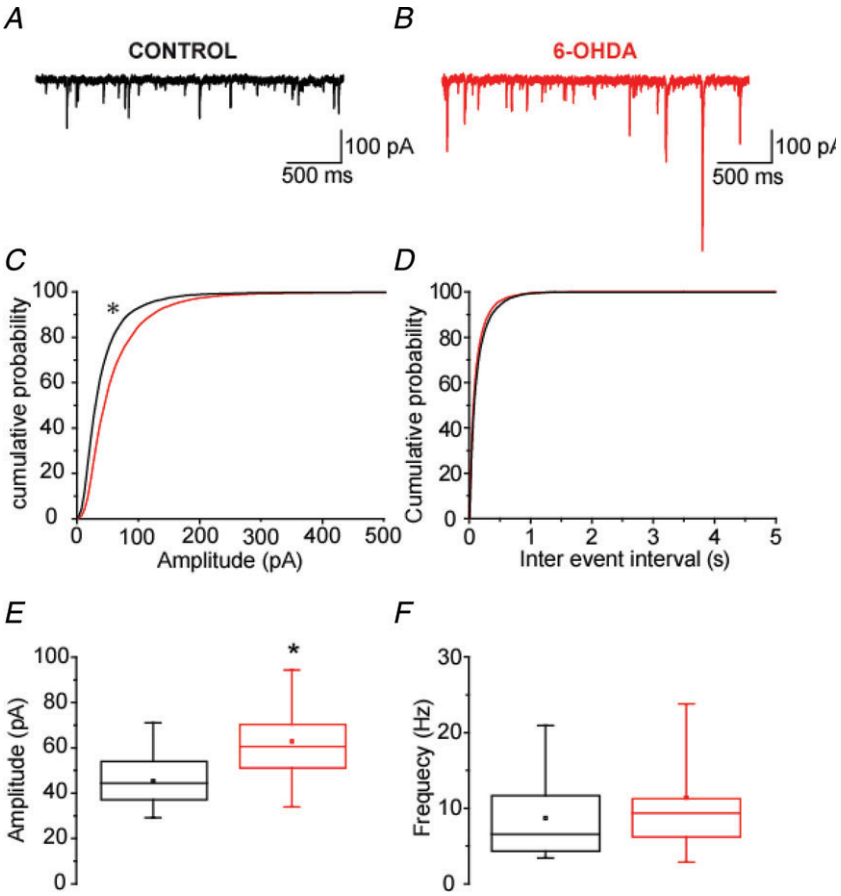

Figure 6. Chronic dopamine depletion increases the amplitude of mIPSCs
A and *B*, representative recordings of mIPSC in GP neurons obtained from control and 6-OHDA animals. *C* and *D*, cumulative probability plots of the sample populations showed that dopamine depletion significantly increased the amplitude of mIPSCs (control, $n = 13$; 6-OHDA, $n = 12$; $P < 0.01$; K-S test) and had no effect on their frequency. *E* and *F*, box plots showing that the mean amplitude of mIPSCs was significantly increased (control, $n = 13$; 6-OHDA, $n = 12$; $P = 0.015$; MW *U* test) whereas the mean frequency remained unchanged.

Finally, we compared the capacity of a high-frequency train (25 pulses; 50 Hz) to trigger a rebound burst. Such a train of IPSPs silenced the activity of the recorded neurons both in control and in dopamine-depleted conditions, but evoked post-inhibitory rebound only in 6-OHDA treated animals (Fig. 9*F* and *G*). Rebounds obtained under dopamine-depleted conditions were characterized by a significant 32% increase ($P = 0.003$, MW *U* test) in the

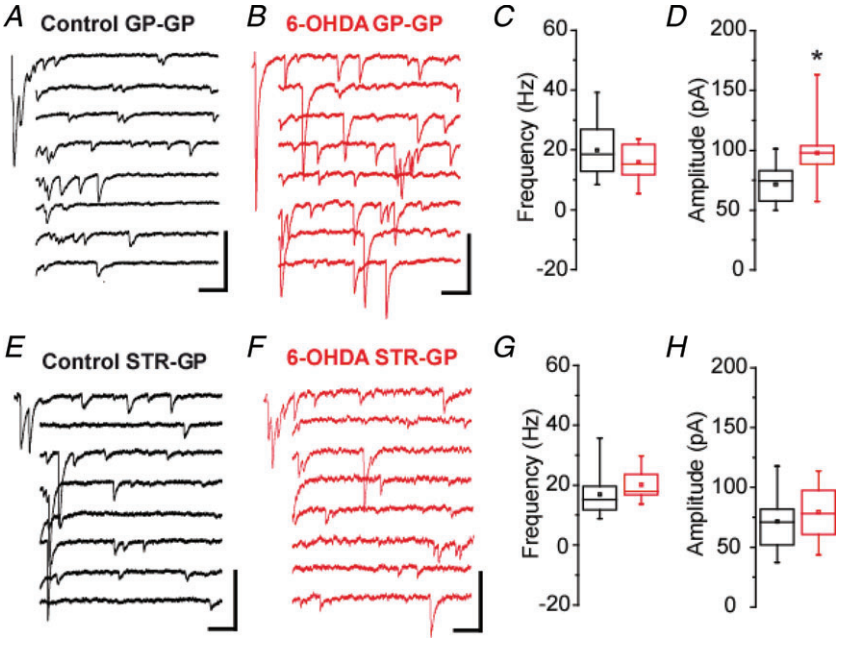

Figure 7. Chronic dopamine depletion increases the amplitude of quantal-like IPSCs only at putative GP–GP synapses in Sr^{2+}-induced asynchronous release recording conditions
A, examples of Sr^{2+}-induced asynchronous qIPSCs evoked after pallidal electrical stimulation in a coronal slice from a control animal. *B*, same as *A* for a 6-OHDA-lesioned animal. *C* and *D*, box plots illustrating the qIPSC frequency (*C*) and amplitude (*D*) in control (black box plots) and dopamine-depleted slices (red box plots; grey in the print edition). Control, $n = 11$; 6-OHDA, $n = 9$; $P = 0.023$, MW *U* test. *E*, examples of Sr^{2+}-induced asynchronous qIPSCs evoked after striatal electrical stimulation in a parasagittal slice from a control animal. *F*, same as *E* for a 6-OHDA-lesioned animal. *G* and *H*, box plots illustrating the qIPSC frequency (*G*) and amplitude (*H*) in control (black box plots) and dopamine-depleted slices (red box plots; grey in the print edition).

post-IPSP firing frequency (Fig. 9*G* inset). Altogether, these data suggest that an increase in the potency of GP–GP GABAergic transmission has a strong impact on the resetting of autonomous pacemaking and the patterning of GP neuron activity.

Discussion

The main finding of this study is that chronic dopamine depletion induces a postsynaptic increase in the potency of GP–GP GABAergic transmission (i.e. intranuclear inhibition) which participates to the altered activity of GP neurons.

In the present study we found that STR–GP and GP–GP synapses have distinctive properties. The STR–GP pathway has been characterized *in vitro* (Cooper & Stanford, 2001; Sims *et al.* 2008; Chuhma *et al.* 2011). Here, we provide additional evidence showing that STF is a specific signature of this synapse using pathway-specific photostimulation of ChR2-expressing MSNs. This mode of synaptic transmission seems to be a common feature of striato-fugal synapses (both direct and indirect pathways) as striato-nigral synapses are also governed by STF (Connelly *et al.* 2010). The optogenetic approach was particularly important to exclude that depressing responses recorded by electrical stimulation of the striatum in parasagittal slices would correspond to activation of STR–GP inputs. As approximately 1/3 of pallidal neurons project back to the striatum (Bevan *et al.* 1998), it is likely that depressing responses correspond to antidromic activation of pallido-striatal neurons. The insensitivity of these responses to D_2R modulation further suggests that depressing IPSCs recorded in parasagittal and coronal slices reflect the activity of GP–GP synapses. In target nuclei of pallidal neurons such as the STN and substantia nigra pars reticulata, STD is also a characteristic of pallido-subthalamic and pallido-nigral GABAergic transmission (Baufreton & Bevan, 2008; Connelly *et al.* 2010).

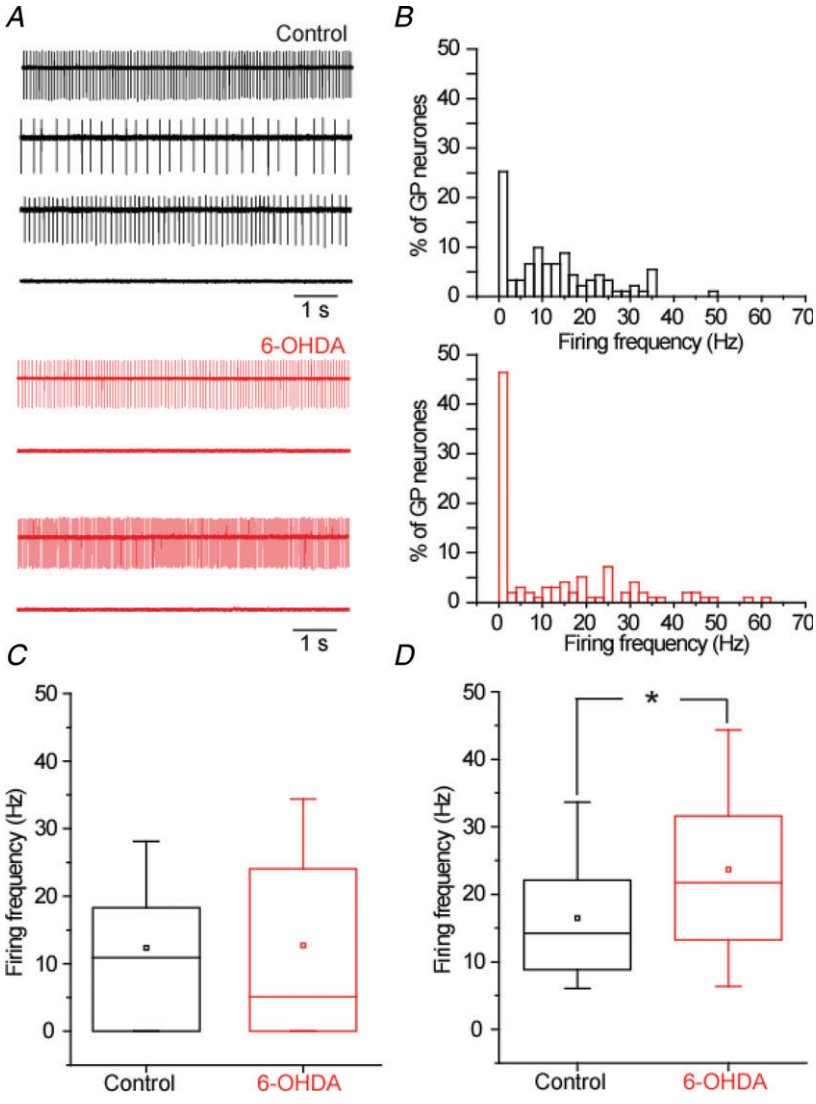

Figure 8. Chronic dopamine depletion induces a bi-directional modification of autonomous pacemaking in GP neurons
A, representative examples of cell-attached recordings of GP neurons derived from control and 6-OHDA lesioned animals. *B*, histograms of firing rate for control and 6-OHDA cell populations. *C*, box plots of mean firing rate (control, $n = 91$; 6-OHDA, $n = 97$; $P = 0.292$; MW *U* test). *D*, box plots of mean firing including only spiking GP neurons (control, $n = 68$; 6-OHDA, $n = 52$; $P = 0.004$; MW *U* test).

Dopamine has complex effects on the activity of GP neurons *in vivo* (Ruskin *et al.* 1998, 1999; Dejean *et al.* 2011) probably because it acts on both presynaptic and postsynaptic elements, thereby controlling synaptic weight and neuronal excitability (Cooper & Stanford, 2001; Stefani *et al.* 2002). D_2R stimulation reduces GABA release from STR–GP synapses (Cooper & Stanford, 2001) whereas D_4R diminishes $GABA_A$ synaptic current amplitude by postsynaptic modulation of $GABA_A$ receptor function (Shin *et al.* 2003). According to the classical model of the basal ganglia, the STR–GP indirect pathway is hyperactive after dopaminergic denervation (Alexander & Crutcher, 1990). Surprisingly, our data suggest that STR–GP synapses are not impacted in their functioning after chronic dopamine depletion, which contrasts with the dramatic increase in STR–GP synapse size reported in 6-OHDA-lesioned rats (Ingham *et al.* 1997). This result may explain why therapeutical strategies targeting STR–GP synapse efficacy have a limited impact on PD motor symptoms (Black *et al.* 2010; Hauser, 2011).

Although several reports suggest that some GP neurons express D_2-like dopamine receptors (Stefani *et al.* 2002; Hoover & Marshall, 2004; Araki *et al.* 2007), we found that D_2Rs do not modulate GP–GP synaptic transmission,

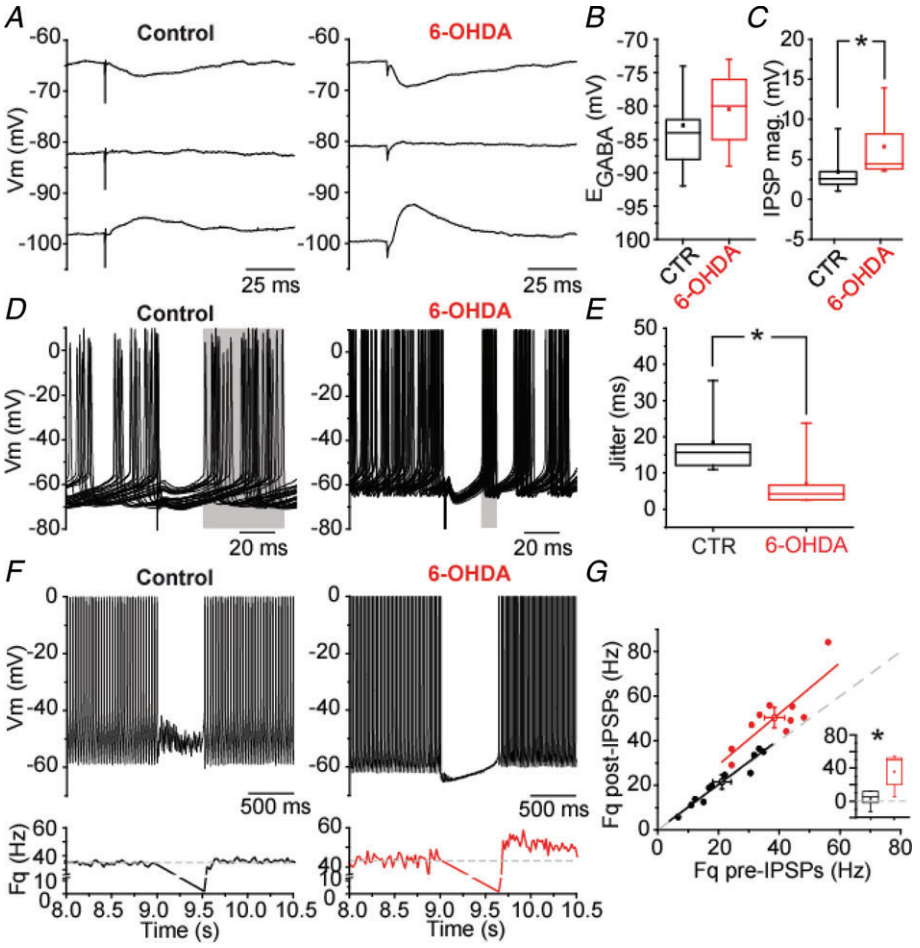

Figure 9. Increased GP–GP inhibition resets more efficiently autonomous pacemaking and promotes rebound-burst firing
A, representative examples of GABAergic IPSPs evoked at various membrane potential. *B*, graph depicting $GABA_A$ receptor-mediated IPSP reversal potential (E_{GABA}; control, $n = 9$; 6-OHDA, $n = 9$; $P = 0.289$, MW *U* test). *C*, plot showing the significant increase in the magnitude of IPSPs in dopamine-depleted conditions measured at a potential of −65 mV (control, $n = 9$; 6-OHDA, $n = 6$; $P = 0.039$, MW *U* test). *D*, plots illustrating the impact of single IPSP in the resetting of GP neuron autonomous pacemaking (overlay of 30 traces in each conditions). *E*, graph representing the jitter of the action potential following the IPSP (control, $n = 5$; 6-OHDA, $n = 7$; $P = 0.03$, MW *U* test). *F*, examples of the effect of a train of IPSP (25 pulses; 50 Hz) on GP neurons firing. The graph below each trace indicates the modification of instantaneous frequency. The dash lines indicate the mean firing frequency before the train of evoked IPSPs. *G*, correlation graph between the pre-IPSP firing frequency (measured over a duration of 500 ms) and the post-IPSP firing frequency (measured over a duration of 300 ms). Inset, summary graph showing the significant change in post-IPSP firing frequency in dopamine-depleted conditions (control, $n = 11$; 6OHDA, $n = 10$; $P = 0.003$, MW *U* test).

emphasizing that intranuclear inhibition in the GP is not regulated by the D_2-like receptor family. One possible explanation for this apparent discrepancy could be that D_2-like receptors are not trafficked to pre-synaptic GP axon terminals but remain restricted to the somato-dendritic compartment of GP neurons. Therefore, the increase in synaptic weight of this connection in dopamine-depleted animals would not result from the loss of the dopaminergic modulation of this pathway. An alternative and compatible explanation for this change in efficacy is a maladaptive homeostasis in response either (1) to the complex alteration of GP neurons excitability in experimental PD (Chan *et al.* 2011; this study), or (2) to the hyperactivity of the STN commonly reported in dopamine-depleted animals (Bergman *et al.* 1994; Magill *et al.* 2001). In the latter case, the mechanism involved in the potentiation of GABA transmission could be an NMDAR-dependent increase in $GABA_A$ receptor membrane expression (Marsden *et al.* 2007).

Using Sr^{2+}-induced asynchronous release of GABA, we showed that the increase in quantal amplitude contributes to enhanced GP–GP transmission in 6-OHDA rats. This result disagrees with the reduced expression of $GABA_A$ receptor subunits reported in a dopamine-depleted state in the GP (Caruncho *et al.* 1997; Chadha *et al.* 2000). The most cautious explanation for this discrepancy is that this global reduction in $GABA_A$ sub-unit membrane expression masks a local somatic increase in $GABA_A$ receptor expression or function specific for GP–GP synapses. $GABA_A$ receptors are knowingly the targets of intracellular dopamine signalling pathways leading to the control of synaptic strength, either by direct phosphorylation/dephosphorylation (Poisbeau *et al.* 1999) or by a reduction in the traffic and the clustering of $GABA_A$ receptor (Graziane *et al.* 2009). Loss of these modulatory pathways in dopamine-depleted conditions might contribute to the upregulation of GABAergic transmission we report at GP–GP synapses.

Basal ganglia undergo profound alterations in PD both at cellular and synaptic levels (Bevan *et al.* 2002; Hammond *et al.* 2007), which are believed to participate in the generation of a pathological synchronous pattern of activity and contribute to the emergence of the symptoms of the disease (Hutchison *et al.* 2004). At the GP level, autonomous pacemaking has been shown to be markedly reduced in experimental models of PD (Chan *et al.* 2011). Our results are only partially supportive of this finding as we did observe an increase in the percentage of silent GP neurons after chronic dopamine depletion. However, we also found that the remaining active GP neurons fired action potentials at a higher rate than GP neurons from naive animals. The reason for this discrepancy may depend on the number of cells included in each study. In the present study a substantially greater number of GP neurons were recorded under chronic dopamine-depletion and thus the analysed sample reflects more accurately the heterogeneity of GP neurons. The bi-directional change in excitability reported here could be related to the loss of a direct dopaminergic modulation of the D_2R-expressing GP neurons (Hoover & Marshall, 2004) combined with compensatory mechanisms in the other neuronal population.

Because the GP sends widespread connections to the entire network, the increase in potency of GABAergic pallido-fugal synapses (including GP–GP lateral inhibition) in Parkinson-like conditions could work as an amplifier of oscillatory activity by (1) enhancing cortically-driven beta-oscillations (Baufreton *et al.* 2005) or rebound bursting (Hallworth & Bevan, 2005; Baufreton & Bevan, 2008) in the STN, and (2) producing an imbalance in GABAergic inhibition within the GP and contributing to the abnormal and inversely related pattern of activity of clusters of GP neurons observed in dopamine-depleted rodents (Filion & Tremblay, 1991; Mallet *et al.* 2008). Finally, our data complete recent reports (Day *et al.* 2006; Chan *et al.* 2011; Gittis *et al.* 2011) supporting the conclusion that maladaptive intrinsic cellular and synaptic plasticity mechanisms take place along the elements of the indirect pathway of the basal ganglia and contribute to pathological activity in GP neurons and hence in the entire basal ganglia network in PD.

References

Ahmed MR, Berthet A, Bychkov E, Porras G, Li Q, Bioulac BH, Carl YT, Bloch B, Kook S, Aubert I, Dovero S, Doudnikoff E, Gurevich VV, Gurevich EV & Bezard E (2010). Lentiviral overexpression of GRK6 alleviates L-dopa-induced dyskinesia in experimental Parkinson's disease. *Sci Transl Med* **2**, 28ra28.

Alexander GE & Crutcher MD (1990). Functional architecture of basal ganglia circuits: neural substrates of parallel processing. *Trends Neurosci* **13**, 266–271.

Araki KY, Sims JR & Bhide PG (2007). Dopamine receptor mRNA and protein expression in the mouse corpus striatum and cerebral cortex during pre- and postnatal development. *Brain Res* **1156**, 31–45.

Barry PH (1994). JPCalc, a software package for calculating liquid junction potential corrections in patch-clamp, intracellular, epithelial and bilayer measurements and for correcting junction potential measurements. *J Neurosci Methods* **51**, 107–116.

Baufreton J, Atherton JF, Surmeier DJ & Bevan MD (2005). Enhancement of excitatory synaptic integration by GABAergic inhibition in the subthalamic nucleus. *J Neurosci* **25**, 8505–8517.

Baufreton J & Bevan MD (2008). D2-like dopamine receptor-mediated modulation of activity-dependent plasticity at GABAergic synapses in the subthalamic nucleus. *J Physiol* **586**, 2121–2142.

Bergman H, Wichmann T, Karmon B & DeLong MR (1994). The primate subthalamic nucleus. II. Neuronal activity in the MPTP model of parkinsonism. *J Neurophysiol* **72**, 507–520.

Bevan MD, Booth PA, Eaton SA & Bolam JP (1998). Selective innervation of neostriatal interneurons by a subclass of neuron in the globus pallidus of the rat. *J Neurosci* **18**, 9438–9452.

Bevan MD, Magill PJ, Terman D, Bolam JP & Wilson CJ (2002). Move to the rhythm: oscillations in the subthalamic nucleus-external globus pallidus network. *Trends Neurosci* **25**, 525–531.

Bevan MD, Wilson CJ, Bolam JP & Magill PJ (2000). Equilibrium potential of $GABA_A$ current and implications for rebound burst firing in rat subthalamic neurons in vitro. *J Neurophysiol* **83**, 3169–3172.

Bezard E, Dovero S, Bioulac B & Gross CE (1997). Kinetics of nigral degeneration in a chronic model of MPTP-treated mice. *Neurosci Lett* **234**, 47–50.

Black KJ, Koller JM, Campbell MC, Gusnard DA & Bandak SI (2010). Quantification of indirect pathway inhibition by the adenosine A2a antagonist SYN115 in Parkinson disease. *J Neurosci* **30**, 16284–16292.

Caruncho HJ, Liste I, Rozas G, Lopez-Martin E, Guerra MJ & Labandeira-Garcia JL (1997). Time course of striatal, pallidal and thalamic α_1, α_2 and $\beta_{2/3}$ $GABA_A$ receptor subunit changes induced by unilateral 6-OHDA lesion of the nigrostriatal pathway. *Brain Res Mol Brain Res* **48**, 243–250.

Cenci MA & Lundblad M (2007). Ratings of L-DOPA-induced dyskinesia in the unilateral 6-OHDA lesion model of Parkinson's disease in rats and mice. *Curr Protoc Neurosci* Chapter 9, Unit 9.25.

Chadha A, Dawson LG, Jenner PG & Duty S (2000). Effect of unilateral 6-hydroxydopamine lesions of the nigrostriatal pathway on $GABA_A$ receptor subunit gene expression in the rodent basal ganglia and thalamus. *Neuroscience* **95**, 119–126.

Chan CS, Glajch KE, Gertler TS, Guzman JN, Mercer JN, Lewis AS, Goldberg AB, Tkatch T, Shigemoto R, Fleming SM, Chetkovich DM, Osten P, Kita H & Surmeier DJ (2011). HCN channelopathy in external globus pallidus neurons in models of Parkinson's disease. *Nat Neurosci* **14**, 85–92.

Chuhma N, Tanaka KF, Hen R & Rayport S (2011). Functional connectome of the striatal medium spiny neuron. *J Neurosci* **31**, 1183–1192.

Connelly WM, Schulz JM, Lees G & Reynolds JN (2010). Differential short-term plasticity at convergent inhibitory synapses to the substantia nigra pars reticulata. *J Neurosci* **30**, 14854–14861.

Cooper AJ & Stanford IM (2001). Dopamine D2 receptor mediated presynaptic inhibition of striatopallidal $GABA_A$ IPSCs in vitro. *Neuropharmacology* **41**, 62–71.

Cruikshank SJ, Urabe H, Nurmikko AV & Connors BW (2010). Pathway-specific feedforward circuits between thalamus and neocortex revealed by selective optical stimulation of axons. *Neuron* **65**, 230–245.

Davidson BL & Breakefield XO (2003). Viral vectors for gene delivery to the nervous system. *Nat Rev Neurosci* **4**, 353–364.

Day M, Wang Z, Ding J, An X, Ingham CA, Shering AF, Wokosin D, Ilijic E, Sun Z, Sampson AR, Mugnaini E, Deutch AY, Sesack SR, Arbuthnott GW & Surmeier DJ (2006). Selective elimination of glutamatergic synapses on striatopallidal neurons in Parkinson disease models. *Nat Neurosci* **9**, 251–259.

Dejean C, Arbuthnott G, Wickens JR, Le Moine C, Boraud T & Hyland BI (2011). Power fluctuations in beta and gamma frequencies in rat globus pallidus: association with specific phases of slow oscillations and differential modulation by dopamine D1 and D2 receptors. *J Neurosci* **31**, 6098–6107.

Filion M & Tremblay L (1991). Abnormal spontaneous activity of globus pallidus neurons in monkeys with MPTP-induced parkinsonism. *Brain Res* **547**, 142–151.

Fioravante D & Regehr WG (2011). Short-term forms of presynaptic plasticity. *Curr Opin Neurobiol* **21**, 269–274.

Gittis AH, Hang GB, LaDow ES, Shoenfeld LR, Atallah BV, Finkbeiner S & Kreitzer AC (2011). Rapid target-specific remodeling of fast-spiking inhibitory circuits after loss of dopamine. *Neuron* **71**, 858–868.

Goldberg JA, Kats SS & Jaeger D (2003). Globus pallidus discharge is coincident with striatal activity during global slow wave activity in the rat. *J Neurosci* **23**, 10058–10063.

Graziane NM, Yuen EY & Yan Z (2009). Dopamine D4 receptors regulate $GABA_A$ receptor trafficking via an actin/cofilin/myosin-dependent mechanism. *J Biol Chem* **284**, 8329–8336.

Gross CE, Ravenscroft P, Dovero S, Jaber M, Bioulac B & Bezard E (2003). Pattern of levodopa-induced striatal changes is different in normal and MPTP-lesioned mice. *J Neurochem* **84**, 1246–1255.

Hallworth NE & Bevan MD (2005). Globus pallidus neurons dynamically regulate the activity pattern of subthalamic nucleus neurons through the frequency-dependent activation of postsynaptic $GABA_A$ and $GABA_B$ receptors. *J Neurosci* **25**, 6304–6315.

Hammond C, Bergman H & Brown P (2007). Pathological synchronization in Parkinson's disease: networks, models and treatments. *Trends Neurosci* **30**, 357–364.

Hauser RA (2011). Future treatments for Parkinson's disease: surfing the PD pipeline. *Int J Neurosci* **121**(Suppl 2), 53–62.

Hoover BR & Marshall JF (2004). Molecular, chemical, and anatomical characterization of globus pallidus dopamine D2 receptor mRNA-containing neurons. *Synapse* **52**, 100–113.

Hutchison WD, Dostrovsky JO, Walters JR, Courtemanche R, Boraud T, Goldberg J & Brown P (2004). Neuronal oscillations in the basal ganglia and movement disorders: evidence from whole animal and human recordings. *J Neurosci* **24**, 9240–9243.

Ingham CA, Hood SH, Mijnster MJ, Baldock RA & Arbuthnott GW (1997). Plasticity of striatopallidal terminals following unilateral lesion of the dopaminergic nigrostriatal pathway: a morphological study. *Exp Brain Res* **116**, 39–49.

Kita H (1994). Parvalbumin-immunopositive neurons in rat globus pallidus: a light and electron microscopic study. *Brain Res* **657**, 31–41.

Kita H & Kita T (2011). Role of striatum in the pause and burst generation in the globus pallidus of 6-OHDA-treated rats. *Front Syst Neurosci* **5**, 42.

Magill PJ, Bolam JP & Bevan MD (2000). Relationship of activity in the subthalamic nucleus-globus pallidus network to cortical electroencephalogram. *J Neurosci* **20**, 820–833.

Magill PJ, Bolam JP & Bevan MD (2001). Dopamine regulates the impact of the cerebral cortex on the subthalamic nucleus-globus pallidus network. *Neuroscience* **106**, 313–330.

Mallet N, Pogosyan A, Marton LF, Bolam JP, Brown P & Magill PJ (2008). Parkinsonian beta oscillations in the external globus pallidus and their relationship with subthalamic nucleus activity. *J Neurosci* **28**, 14245–14258.

Marsden KC, Beattie JB, Friedenthal J & Carroll RC (2007). NMDA receptor activation potentiates inhibitory transmission through GABA receptor-associated protein-dependent exocytosis of $GABA_A$ receptors. *J Neurosci* **27**, 14326–14337.

Miguelez C, Aristieta A, Cenci MA & Ugedo L (2011*a*). The locus coeruleus is directly implicated in L-DOPA-induced dyskinesia in parkinsonian rats: an electrophysiological and behavioural study. *PLoS One* **6**, e24679.

Miguelez C, Grandoso L & Ugedo L (2011*b*). Locus coeruleus and dorsal raphe neuron activity and response to acute antidepressant administration in a rat model of Parkinson's disease. *Int J Neuropsychopharmacol* **14**, 187–200.

Mink JW & Thach WT (1991). Basal ganglia motor control. I. Nonexclusive relation of pallidal discharge to five movement modes. *J Neurophysiol* **65**, 273–300.

Nini A, Feingold A, Slovin H & Bergman H (1995). Neurons in the globus pallidus do not show correlated activity in the normal monkey, but phase-locked oscillations appear in the MPTP model of parkinsonism. *J Neurophysiol* **74**, 1800–1805.

Poisbeau P, Cheney MC, Browning MD & Mody I (1999). Modulation of synaptic $GABA_A$ receptor function by PKA and PKC in adult hippocampal neurons. *J Neurosci* **19**, 674–683.

Ruskin DN, Bergstrom DA & Walters JR (1999). Multisecond oscillations in firing rate in the globus pallidus: synergistic modulation by D1 and D2 dopamine receptors. *J Pharmacol Exp Ther* **290**, 1493–1501.

Ruskin DN, Rawji SS & Walters JR (1998). Effects of full D1 dopamine receptor agonists on firing rates in the globus pallidus and substantia nigra pars compacta in vivo: tests for D1 receptor selectivity and comparisons to the partial agonist SKF 38393. *J Pharmacol Exp Ther* **286**, 272–281.

Sadek AR, Magill PJ & Bolam JP (2007). A single-cell analysis of intrinsic connectivity in the rat globus pallidus. *J Neurosci* **27**, 6352–6362.

Sato F, Lavallee P, Levesque M & Parent A (2000). Single-axon tracing study of neurons of the external segment of the globus pallidus in primate. *J Comp Neurol* **417**, 17–31.

Schallert T, Fleming SM, Leasure JL, Tillerson JL & Bland ST (2000). CNS plasticity and assessment of forelimb sensorimotor outcome in unilateral rat models of stroke, cortical ablation, parkinsonism and spinal cord injury. *Neuropharmacology* **39**, 777–787.

Shin RM, Masuda M, Miura M, Sano H, Shirasawa T, Song WJ, Kobayashi K & Aosaki T (2003). Dopamine D4 receptor-induced postsynaptic inhibition of GABAergic currents in mouse globus pallidus neurons. *J Neurosci* **23**, 11662–11672.

Sims RE, Woodhall GL, Wilson CL & Stanford IM (2008). Functional characterization of GABAergic pallidopallidal and striatopallidal synapses in the rat globus pallidus in vitro. *Eur J Neurosci* **28**, 2401–2408.

Smith Y, Bevan MD, Shink E & Bolam JP (1998). Microcircuitry of the direct and indirect pathways of the basal ganglia. *Neuroscience* **86**, 353–387.

Stefani A, Spadoni F, Martorana A, Lavaroni F, Martella G, Sancesario G & Bernardi G (2002). D2-mediated modulation of N-type calcium currents in rat globus pallidus neurons following dopamine denervation. *Eur J Neurosci* **15**, 815–825.

Terman D, Rubin JE, Yew AC & Wilson CJ (2002). Activity patterns in a model for the subthalamopallidal network of the basal ganglia. *J Neurosci* **22**, 2963–2976.

Vila M, Perier C, Feger J, Yelnik J, Faucheux B, Ruberg M, Raisman-Vozari R, Agid Y & Hirsch EC (2000). Evolution of changes in neuronal activity in the subthalamic nucleus of rats with unilateral lesion of the substantia nigra assessed by metabolic and electrophysiological measurements. *Eur J Neurosci* **12**, 337–344.

West MJ (1999). Stereological methods for estimating the total number of neurons and synapses: issues of precision and bias. *Trends Neurosci* **22**, 51–61.

Zhang F, Gradinaru V, Adamantidis AR, Durand R, Airan RD, de Lecea L & Deisseroth K (2010). Optogenetic interrogation of neural circuits: technology for probing mammalian brain structures. *Nat Protoc* **5**, 439–456.

Author contributions

C.M. and J.B. designed research; C.M., S.M. and J.B. performed research; A.M. and M.G. contributed reagents/materials/analysis tools; C.M., S.M. and J.B. analyzed data; C.M., E.B., B.B. and J.B. wrote the paper. All authors approved the final version of the manuscript for publication.

Acknowledgements

This research is supported by the French National Research Agency ANR grant 08-JCJC 0087 (J.B.), the region of Aquitaine (J.B.) and the Basque government (C.M. post-doctoral grant). We are grateful to Dr S. Oliet for his help in the design of the strontium-induced asynchronous release of GABA experiments, Dr K. Deisseroth for providing us with the lentivirus channelrhodopsin-2 constructs used for the optogenetic experiments and Dr Anne Taupignon for her critical comments on the manuscript.